Title

Multi-bounce self-mixing in terahertz metasurface external-cavity lasers

Journal

Optics Express, 32(11)

ISSN

1094-4087

Authors

Kim, Anthony D
McGovern, Daniel J
Williams, Benjamin S

Publication Date

2024-05-20

DOI

10.1364/oe.523012

Peer reviewed

To be published in Optics Express:

Title:	Multi-bounce self-mixing in terahertz metasurface external-cavity lasers
Authors:	Anthony Kim,Daniel McGovern,Benjamin Williams
Accepted:	29 April 24
Posted	30 April 24
DOI:	https://doi.org/10.1364/OE.523012

Multi-bounce self-mixing in terahertz metasurface external-cavity lasers

ANTHONY D. KIM,[1,*] DANIEL J. MCGOVERN,[1] AND BENJAMIN S. WILLIAMS[1]

[1] *Department of Electrical and Computer Engineering, University of California, Los Angeles, California 90095, USA*
[*] *dkim95@ucla.edu*

Abstract: The effects of optical feedback on a terahertz (THz) quantum-cascade metasurface vertical-external-cavity surface-emitting laser (QC-VECSEL) are investigated via self-mixing. A single-mode 2.80 THz QC-VECSEL operating in continuous-wave is subjected to various optical feedback conditions (i.e. feedback strength, round-trip time, and angular misalignment) while variations in its terminal voltage associated with self-mixing are monitored. Due to its large radiating aperture and near-Gaussian beam shape, we find that the QC-VECSEL is strongly susceptible to optical feedback, which is robust against misalignment of external optics. This, in addition to the use of a high-reflectance flat output coupler, results in high feedback levels associated with multiple round-trips within the external cavity — a phenomenon not typically observed for ridge-waveguide QC-lasers. Thus, a new theoretical model is established to describe self-mixing in the QC-VECSEL. The stability of the device under variable optical feedback conditions is also studied. Any mechanical instabilities of the external cavity (such as vibrations of the output coupler), are enhanced due to feedback and result in low-frequency oscillations of the terminal voltage. The work reveals how the self-mixing response differs for the QC-VECSEL architecture, informs other systems in which optical feedback is unavoidable, and paves the way for QC-VECSEL self-mixing applications.

1. Introduction

Self-mixing (SM) interferometry within terahertz (THz) quantum-cascade lasers (QCLs) has garnered significant attention in the past decade for various sensing applications. In SM interferometry, the output beam of a laser is intentionally reinjected back into the laser cavity, which coherently perturbs both the amplitude and phase of the intra-cavity field. The reinjected beam contains information regarding its journey, which it then imparts onto the laser's measurable properties such as its power output and terminal voltage. The latter property is particularly useful for sensing, since the response is quite fast, and is fundamentally limited by the relevant laser electron and photon lifetimes (typically tens of picoseconds at most), and the RC-time constants associated with the laser packaging. The sensing is coherent and can be very sensitive, which is particularly useful considering the lack of convenient room-temperature fast detectors in the THz. In this way, sensing applications become achievable using THz QC-lasers without the need for a separate detector. Some of the first set of demonstrations were in THz imaging, where SM was used to perform long distance imaging, real-time imaging, and depth-resolved sensing [1–4]. SM has also been used to demonstrate material characterization, gas spectroscopy, displacement sensing, velocimetry, and near-field microscopy [2, 5–11]. Beyond sensing, SM has been used for laser self-characterization [12–14]. This is because the laser response to optical feedback is dependent on key laser parameters such as the linewidth enhancement factor (LEF), laser linewidth, and the emission spectrum. The LEF in particular has been shown to play a key role in optical frequency comb generation in THz QCLs [15, 16]. Self-mixing is an important tool towards studying the effect that optical feedback can have on the laser itself. Depending on the feedback conditions, and the type of semiconductor laser, optical feedback is known to cause the laser to mode hop, multi-mode, stabilize, destabilize, or even drive the

laser into chaos [17–22]. Due to extremely fast gain recovery times, and near-zero LEFs, QCLs have been shown to be particularly stable under optical feedback compared to semiconductor diode lasers [23]. Nonetheless, optical feedback has been shown to have a significant effect on frequency comb operation and stability in THz QC-lasers [21, 24, 25]. The intentional or accidental presence of feedback must always be considered, since there are no readily available optical isolators in the 1–10 THz range. To date, almost all demonstrations of SM interferometry in THz QCLs has been performed via surface-plasmon waveguide edge-emitting lasers, which were favored over metal-metal waveguide lasers because of their larger waveguide mode, which has eased optical coupling upon retroreflection [26].

In this work, self-mixing in a THz QC vertical-external-cavity surface-emitting laser (QC-VECSEL) is studied for the first time. The QC-VECSEL architecture is based on an amplifying metasurface composed of a periodic sub-wavelength array of microstrip patch antennas loaded with QC gain material [27]. The metasurface, which typically has areas on the order of 1 mm^2, acts as an amplifying mirror in an external Fabry-Pérot cavity with a highly reflective output coupler. This architecture exhibits excellent beam quality, scalable output powers, and the capability for broadband single-mode tuning [28, 29]. Prior to this investigation, it was not immediately obvious how the QC-VECSEL would differ, if at all, from a ridge-waveguide QCL in the context of optical feedback. For example, the VECSEL requires output coupler reflectances typically greater than 90%, which suggests the device may be less sensitive to feedback than an edge-emitting laser with facet reflectance ~30%. At the same time, the large emitting-aperture and the excellent beam-quality favors more efficient coupling. We have already observed the influence of optical feedback in previous experiments on QC-VECSELs, primarily as an unwanted feature. For instance, there was evidence of optical feedback modulating injection locking bandwidths in both optical injection-locking and RF injection-locking schemes, as well as triggering multi-mode oscillation from a nominally single-mode QC-VECSEL [24, 30]. In this work, self-mixing is studied under a variety of experimental conditions, and phenomena unique to the QC-VECSEL architecture are investigated and discussed. Specifically, we observe significant evidence of feedback associated with multiple round-trips within the external cavity. A concise analytical model for self-mixing in the QC-VECSEL is established, which is shown to be in good agreement with experimental data.

2. Theoretical model for multi-bounce self-mixing in THz QC-VECSELs

A theoretical model for self-mixing that includes the effect of the metasurface resonance can be established by adapting the three-mirror model [31]. While a Lang-Kobayashi-based reduced rate equation model can provide a complete time-dependent picture, the three-mirror model can arrive at analytical steady-state solutions that are in good agreement with experiment [14, 21, 32]. This is especially true in THz quantum-cascade lasers because these devices have been shown to remain stable across a wide range of feedback levels [23].

Consider the three-mirror Fabry-Pérot cavity shown in Fig. 1. The reflection coefficients of each mirror are given by Γ_{MS}, Γ_{OC}, and Γ_{ext} respectively. If light transmitted through the output coupler undergoes n round-trips (RTs) in the external feedback cavity, we can write an effective reflection coefficient at the output coupler facet that subsumes the effect of the external cavity:

$$\Gamma_{\text{eff}}(\omega) = \Gamma_{\text{OC}} + (1 - R_{\text{OC}}) \sum_{i=1}^{n} \epsilon_i \Gamma_{\text{OC}}^{i-1} \Gamma_{\text{ext}}^{i} e^{-j2ikL_{\text{ext}}}. \tag{1}$$

If we assume the reflection phases $\phi_{\text{OC}} \approx \phi_{\text{ext}} \approx \pi$, and write

$$\kappa_i = \epsilon_i \left(\frac{1 - R_{\text{OC}}}{R_{\text{OC}}} \right) \left(\sqrt{R_{\text{ext}} R_{\text{OC}}} \right)^i \tag{2}$$

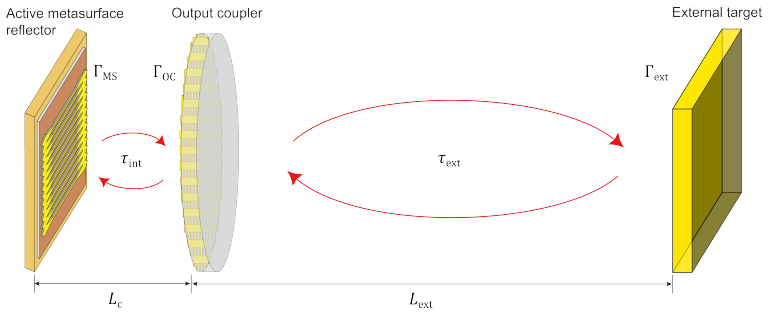

Fig. 1. Schematic of the three-mirror model including the QC-VECSEL. Γ_{MS}, Γ_{OC}, and Γ_{ext} are the reflection coefficients of the metasurface, output coupler, and external target respectively. τ_{int} and τ_{ext} are the internal and external cavity round-trip times. L_c is the VECSEL cavity length, and L_{ext} is the external feedback cavity length.

as the coupling strength associated with the i^{th} RT, we can further write

$$\Gamma_{eff}(\omega) = \sqrt{R_{OC}}e^{j\pi}\left(1 + \sum_{i=1}^{n} \kappa_i e^{-j2ikL_{ext}}\right), \tag{3}$$

where ϵ_i is the total field attenuation in the external cavity, and L_{ext} is the length of the external cavity. We note that these expressions assume an infinitely thin output coupler substrate, but can easily be modified otherwise by including additional phase terms in the exponential. If desired, the reflection phase ϕ_{ext} can be kept general inside the complex exponential to account for arbitrary external targets. Such is the basis for SM sensors for material characterization and analysis [33, 34]. Although the common simplification from this point is to neglect all feedback contributions beyond the first RT ($n = 1$), we find experimentally that this is not a valid approximation for self-mixing in the QC-VECSEL. Thus, we will continue subsequent analyses without loss of generality to n RTs in the external feedback cavity. Based on this result, we can express the resonance condition of the laser cavity as

$$\frac{2\omega L_c}{c} - \phi_{MS}(\omega, n) - \phi_{eff} = 0, \tag{4}$$

where ϕ_{MS} and ϕ_{eff} represent the reflection phase of the metasurface and effective mirror respectively. Comparing this to the resonance condition for the case without external feedback, we can further write

$$0 = \frac{2L_c}{c}\Delta\omega - \Delta\phi_{MS} - \angle\Gamma_{eff}, \tag{5}$$

where $\Delta\omega = \omega - \omega_0$, $\Delta\phi_{MS} = \left[\frac{\partial\phi_{MS}}{\partial\omega}\Delta\omega + \frac{\partial\phi_{MS}}{\partial n}\Delta n\right]\Big|_{\omega_0}$, and ω_0 is the emission frequency of the laser without feedback. Going forward, we make the assumptions $\kappa_i \ll 1$ and that the metasurface reflection coefficient Γ_{MS} is given by a Lorentz oscillator model. We know the first assumption is valid due to the large reflectance of the output coupler ($R_{OC} > \sim 90\%$), as will be shown in Section 4. For the latter assumption, we can see from Fig. 2 that the reflectance and reflection phase of the metasurface obtained via full-wave finite-element (FEM) simulation (COMSOL Multiphysics) matches very closely to an analytical Lorentz oscillator model over its entire bandwidth and for various levels of applied gain. Thus, we can write the metasurface reflection coefficient as

$$\Gamma_{MS} \approx \frac{\frac{1}{4}\left(\tau_r^{-2} - \tau_m^{-2}\right) - (\omega - \omega_r)^2 - j\tau_r^{-1}(\omega - \omega_r)}{\frac{1}{4}\left(\tau_r^{-1} + \tau_m^{-1}\right)^2 + (\omega - \omega_r)^2}, \tag{6}$$

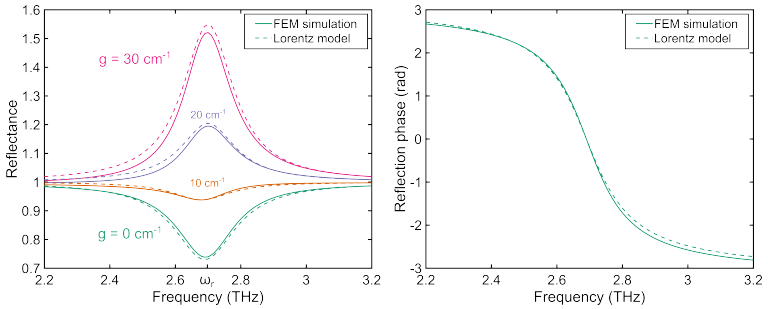

Fig. 2. The metasurface reflectance (left) and reflection phase (right) for the device used in this work. The solid lines are from a full-wave FEM simulation. The dashed lines are based on an analytical Lorentz oscillator model. Reflectance is shown for various levels of applied material gain to compensate for losses.

which provides a reflection phase given by

$$\tan\phi_{\mathrm{MS}} = \frac{\tau_{\mathrm{r}}^{-1}(\omega-\omega_{\mathrm{r}})}{(\omega-\omega_{\mathrm{r}})^2 - \frac{1}{4}\left(\tau_{\mathrm{r}}^{-2}-\tau_{\mathrm{m}}^{-2}\right)}, \tag{7}$$

where τ_{r} is the photon lifetime associated with the radiative loss of the metasurface itself, τ_{m} is the photon lifetime associated with the material loss, and ω_{r} is the resonant frequency of the metasurface.

Plugging everything back into Eq. 5, we arrive at an intuitive form of the phase equation:

$$0 = \tau_{\mathrm{int}}\Delta\omega + \underbrace{\left(\sum_{i=1}^{n}\kappa_i \sin(2ikL_{\mathrm{ext}})\right)}_{\text{FM term}} + \underbrace{\frac{\omega_{\mathrm{r}}}{\omega_0}\alpha\left(\sum_{i=1}^{n}\kappa_i \cos(2ikL_{\mathrm{ext}})\right)}_{\text{AM term}}, \tag{8}$$

where α is the linewidth enhancement factor (LEF) of the material due to the coupling between the index and gain enforced by the Kramers-Kronig relation, and τ_{int} is the RT time of the VECSEL cavity. The first term on the rhs is associated with the RT time of the VECSEL cavity. In general, the RT time includes the group delay associated with the metasurface dispersion. If we assume $\tau_r^{-1} \gg \tau_m^{-1}$, which is typically true since the metasurface is deliberately designed to have a low radiative quality factor, we can write

$$\tau_{\mathrm{int}} = \frac{2L_{\mathrm{c}}}{c} + 2\pi\mathcal{L}(\omega_0) + 2\pi\mathcal{L}(\omega_0)\frac{\omega_{\mathrm{r}}}{n}\frac{\partial n}{\partial\omega}, \tag{9}$$

where $\mathcal{L}(\omega)$ is the Lorentzian lineshape given by

$$\mathcal{L}(\omega) = \frac{1}{2\pi}\frac{\tau_r^{-1}}{(\omega-\omega_{\mathrm{r}})^2 + \frac{1}{4}\tau_r^{-2}}. \tag{10}$$

The second term is the phase contribution from the feedback-induced frequency-modulation (FM) of the laser. The third term is the phase contribution from the feedback-induced amplitude-modulation (AM) of the laser. Note that this term is a consequence of a finite LEF which results in an amplitude-phase coupling inside the oscillator and is an integral part of self-mixing phenomena. However, the factor $\omega_{\mathrm{r}}/\omega_0$ in the AM term is not a factor that appears in conventional ridge lasers, but appears in the VECSEL analysis due to the single-mode detunability away from the metasurface peak reflectance via the Fabry-Pérot VECSEL cavity mode. This detuning

factor contributes to an effective linewidth enhancement factor of the laser which we define as $\alpha_{\text{eff}} \coloneqq (\omega_r/\omega_0)\alpha$. This dependence is not unique to the VECSEL, and is a result of the frequency dependence of the LEF due to the odd-symmetric phase profile [35,36]. In fact, the material LEF is itself also frequency dependent, and so the full dependence on α_{eff} with detuning is not known.

Defining $\phi_{\text{FB}} \coloneqq \omega\tau_{\text{ext}}$ and $\phi_0 \coloneqq \omega_0\tau_{\text{ext}}$, Eq. (8) can be rearranged into the more practical and familiar form of the generalized Adler phase equation,

$$0 = \phi_{\text{FB}} - \phi_0 + \sum_{i=1}^{n} \left[C_i \sin\left(i\phi_{\text{FB}} + \arctan(\alpha_{\text{eff}})\right)\right], \tag{11}$$

where

$$C_i = \kappa_i \sqrt{1+\alpha_{\text{eff}}^2}\frac{\tau_{\text{ext}}}{\tau_{\text{int}}}. \tag{12}$$

For a single RT, the parameter C_i reduces to the familiar Acket parameter, C, which subsumes the various feedback variables and can succinctly describe the regimes of operation of a self-mixing system [37,38]. Therefore, the parameter C_i is an extension of the Acket parameter that describes the feedback level associated with the i^{th} RT of the external cavity. While Eq. (11) describes the perturbation of the emission frequency due to feedback, the SM signal can be obtained from the terminal voltage V_{SM} of the laser at constant current injection due to the modulation of the threshold gain. If we assume the total gain is proportional to the carrier concentration relative to threshold, then

$$V_{\text{SM}} \propto -\frac{2}{\xi}\sum_{i=1}^{n} \kappa_i \cos(i\phi_{\text{FB}}), \tag{13}$$

where ξ is an effective gain interaction length per RT of the VECSEL cavity. Note that this is also a frequency dependent quantity given by $\xi = (c/n)2\pi\mathcal{L}(\omega)$, since it follows from the Lorentzian lineshape of the metasurface amplification.

Some illustrative examples of the relation provided in Eq. (11) are shown in Fig. 3. In particular, we demonstrate the relationship between ϕ_{FB} and ϕ_0 for the case of $n = 2$ and varying C_2 for a given C_1. Fig. 3(a) illustrates the case for $C_1 = 0$, and Fig. 3(b) shows the case for $C_1 = 1$. If we only consider reflections from the second RT, the self-mixing dynamics resemble the conventional case, but with two main distinctions. One, the periodicity is cut by half, resulting in a period of π. In an optical system such as that of Fig. 1, this will manifest as a $\lambda/4$ spatial periodicity of the self-mixing fringes as the external target is translated. Two, the phase relation steps into the regime of multistability sooner than the case of a single RT, resulting in a bistable regime for $0.5 < C_2 < 2.3$. The presence of multiple RTs in the self-mixing analysis precludes the simple delineation of feedback regimes based on a single feedback parameter [39–42]. Thus, for the purposes of this work, we classify the weak feedback regime as the set of C_i n-tuples that maintain bijectivity of the phase relation in Eq. (11). The case for $n = 2$ is illustrated in Fig. 3(c). As ϕ_{FB} becomes multi-valued, the system enters the moderate feedback regime, typically characterized by mode-hopping instabilities, multimoding, and hysteresis [15,17,20].

A few representative self-mixing voltage waveforms according to Eq. (13) are calculated in Fig. 4 for the case of $n = 2$. Fig. 4(a) shows the case for $\alpha = 0$, and Fig. 4(b) shows the case for $\alpha = 0.5$. When both C_1 and C_2 are present, the self-mixing waveform features fringes that don't necessarily peak at the same value. This is indicative of the multi-bounce self-mixing effect and is experimentally demonstrated in Section 4. As the feedback strength gets larger, the waveform develops discontinuities associated with the path-dependence of ϕ_{FB} with respect to ϕ_0. Additionally, comparing Fig. 4(a) and 4(b) illustrates the effect of the LEF on the SM signal morphology; a non-zero α breaks the symmetry and produces a tilt to the signal.

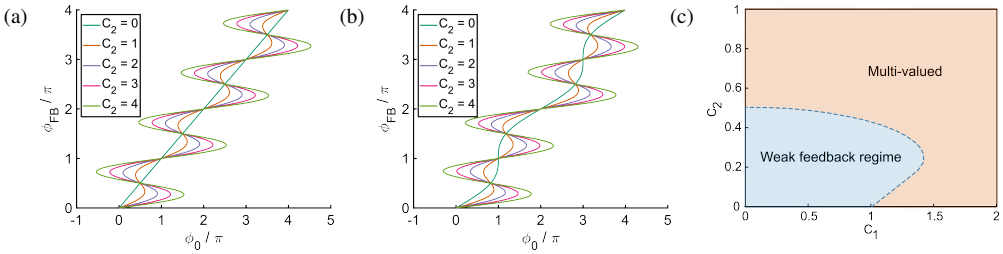

Fig. 3. (a) Feedback phase relation for $C_1 = 0$, and varying C_2 from 0 to 4. (b) Feedback phase relation for $C_1 = 1$, and varying C_2 from 0 to 4. (c) Mapping of the weak feedback regime in the C_1-C_2 plane. Outside this regime, the phase relation becomes multi-valued and enters the moderate feedback regime.

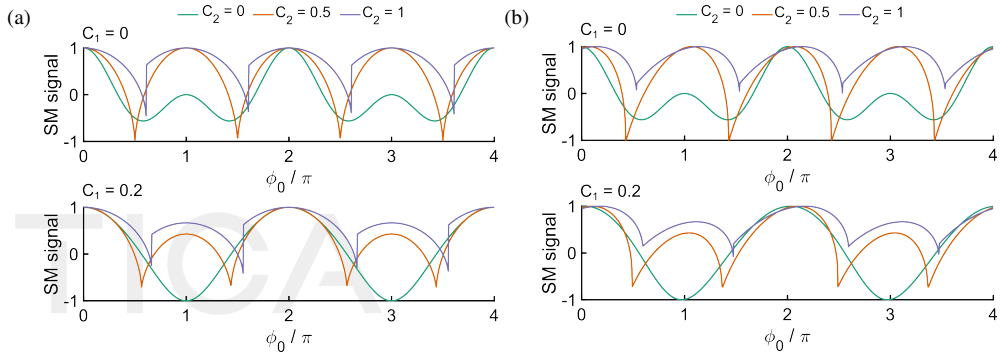

Fig. 4. (a) Calculated SM voltage signals for $C_1 = 0$ and $C_1 = 0.2$ as C_2 is varied and $\alpha_{\text{eff}} = 0$. (b) Same as (a) but for $\alpha_{\text{eff}} = 0.5$.

3. Methods

The QC-VECSEL used in this work is based on an elliptical patch metasurface that couples to surface-incident radiation. The electric field profile of a unit cell is illustrated in Fig. 5(a). The patches are composed of 5-µm-thick QC gain material based on a 4-well phonon-depopulation design grown by IQE plc and was featured in Ref. [43]. The epitaxial growth is 80 repetitions of the layer sequence given, in Å, by 106/**20**/106/**37**/88/**40**/172/**51** (GaAs/$\mathbf{Al_{0.15}Ga_{0.45}As}$), where the middle 88 Å of the underlined layer is nominally doped at 5×10^{16} cm^{-3}. A microscope image of the entire metasurface and a corresponding SEM image of a single patch are shown in Fig. 5(b). The period of the patch array is 50 µm, and the major and minor axes of the ellipse are 21.4 µm and 14.6 µm respectively. Only patches within a central circular area with a diameter of 0.75 mm are biased, so as to preferentially pump the fundamental Gaussian mode of the VECSEL cavity. The output coupler is based on a metallic mesh evaporated on a quartz substrate to give a reflectance of $|\Gamma_{\text{OC}}|^2 = 0.95$. The output coupler is fixed and clamped onto the metasurface die copper submount with a 1 mm thick copper spacer, which eliminates any instabilities or thermal drift associated with a kinematic mount. The laser has a single mode emission peak at 2.80 THz and peak output power of 0.5 mW with threshold current of 385 mA and max current of 460 mA (Fig. 5(c)). The laser is driven in continuous-wave mode by a low noise (3 nA/$\sqrt{\text{Hz}}$) current source from Wavelength Electronics (QCL OEM1000+) and is cooled with liquid nitrogen to 77 K inside a cryostat with a TPX window.

Light leaving the laser is collimated by a 4" focal length f/2 off-axis parabolic (OAP) mirror and reflects off a flat mirror mounted on a 25 mm translation stage, allowing for stepping the

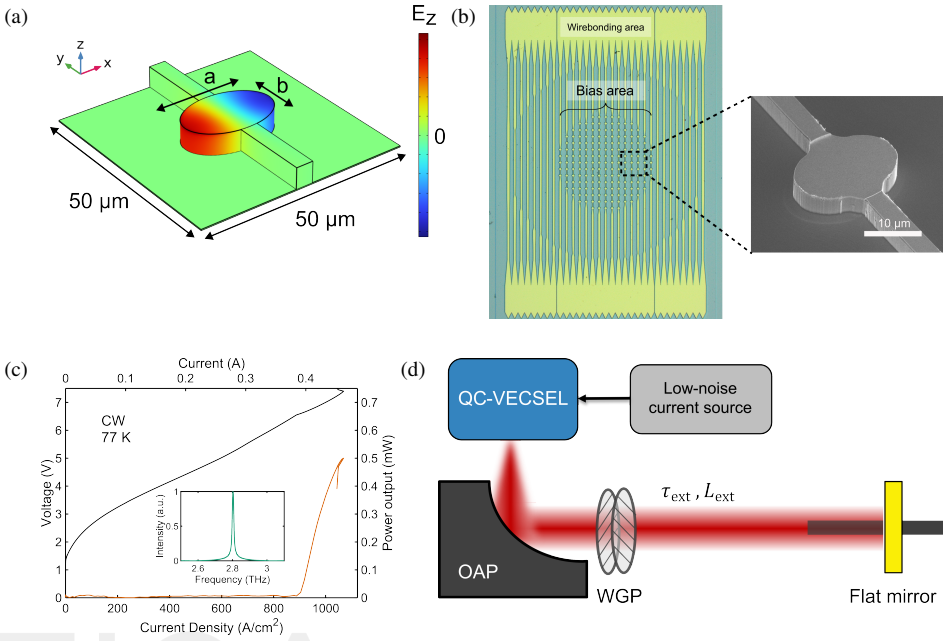

Fig. 5. (a) Simulated electric field profile of the metasurface unit cell. The period of the metasurface is 50 µm in both x and y dimensions. The dimensions of the ellipse are given by a = 21.4 µm and b = 14.6 µm. (b) Optical microscope image of the full metasurface, and an SEM image of a single patch. The patches are selectively biased in a circular bias area in the center of the metasurface. (c) Power-current-voltage measurement of the device under test in continuous-wave operation at 77 K. The inset shows the emission spectrum obtained from an FTIR. (d) Schematic of the experimental setup. Crossed wire-grid polarizers are used whenever additional attenuation is desired.

external cavity length. Moving the translation stage along a fixed rail mount allows for cavity extension from 10 to 80 cm while maintaining the alignment between the two mirrors. The laser emission frequency being near the edge of an atmospheric transmission window necessitates the use of a nitrogen purge enclosure in which relative humidity is reduced to ~1%. Dual wire-grid polarizers (Microtech G30-S) in the collimated beam path are used whenever additional attenuation is desired.

As the translation stage reduces the external cavity length, the SM signal can be recorded as the ac component of the QCL terminal voltage. This signal can be simply acquired using a benchtop multimeter, as was done for the results in Section 4.1. We also employed the conventional method of lock-in detection with an optical chopper (modulated at 200 Hz), which was used for data presented in Section 4.2. However, as will be discussed in Section 4.3, these measurements were accompanied by unexpectedly large noise at higher feedback levels. In response we employed an alternate method, detailed in Section 4.4, involving lock-in differential resistance detection made using small-signal modulation of the current source with a 100 kHz sinusoidal signal.

4. Experimental results

4.1. Multi-bounce self-mixing voltage signal

Without any intentional effort to produce the phenomenon, the experimentally observed SM voltage signal consistently demonstrated feedback coupling from light that underwent two RTs in the external cavity. In fact, when the external cavity length was made sufficiently short

(L_{ext} < 40 cm), we observed SM signals that were dominated by the second RT ($C_2 \gg C_1$). An example of such a signal is shown in Fig. 6(a) for a cavity length of 17.8 cm. Fitting the data to Eq. (11) and Eq. (13) with appropriate normalization, we obtain $C_2 = 0.56 \pm 0.09$ and $\alpha_{eff} = 0.8 \pm 0.3$. The value of α_{eff} is consistent with previously reported SM measurements of the LEF in THz QCLs, ranging from −0.2 to +1 [8, 12].

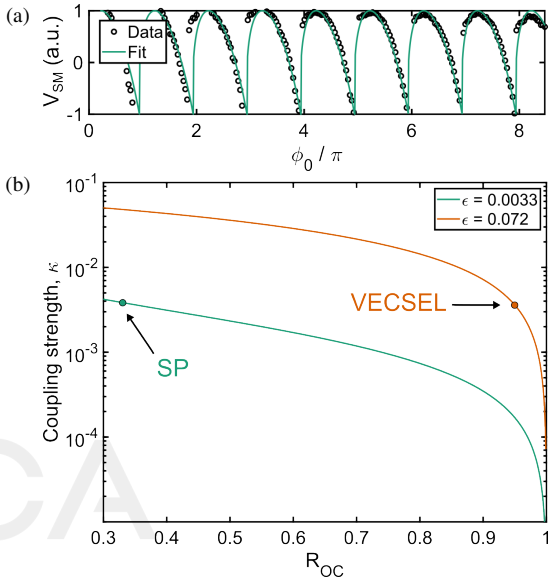

Fig. 6. (a) Normalized SM voltage signal. The green curve is a fit to the collected data based on Eq. (11) and Eq. (13). The extracted parameters are $C_1 \approx 0$, $C_2 = 0.56 \pm 0.09$, and $\alpha_{eff} = 0.8 \pm 0.3$. (b) Coupling strength, κ, versus output coupler reflectance. The green curve corresponds to a surface-plasmon waveguide laser. The orange curve corresponds to the QC-VECSEL. The labeled points show exactly the point of operation.

Based on the fit parameters, we can quantify both the total field attenuation, ϵ, and the coupling strength using Eq. (12). The attenuation factor includes loss from the cryostat window, diffraction, and the mismatch of the spatial mode of the reinjected field. The internal RT time can be calculated from the known laser cavity length (L_c = 1.0 mm) and the simulated metasurface group delay. We obtain an attenuation coefficient of $\epsilon \approx 0.072$, which results in a coupling strength of 3.6×10^{-3}. A recent work by Keeley et al. reported an attenuation coefficient of $\epsilon = 0.0033$ when using a SP waveguide emitting at 3.4 THz [44]. Assuming a facet reflectivity of 33%, the obtained coupling strength is 3.8×10^{-3} — almost identical to that obtained with the VECSEL [45]. At first, the large output coupler reflectances required for the VECSEL might suggest the architecture is not well-suited for SM interferometry. However, the high beam-quality does well to compensate by reducing the amount of reinjected power lost to diffraction and modal-mismatch. Fig. 6(b) illustrates this by comparing the κ vs R_{OC} curves for the respective attenuation coefficients for the SP waveguide and the VECSEL. In fact, while the maximum achievable κ for the SP waveguide is fixed, the VECSEL has some freedom in moving along this curve. VECSELs with OC reflectance as low as 82% have been demonstrated, which would correspond to $\kappa = 1.3 \times 10^{-2}$ [46]. Conversely, the reflectance can be made to be larger to reduce the laser's sensitivity to optical feedback.

4.2. *Asymmetric cavity test*

The observation of multiple RTs in the external cavity as shown in Section 4.1 warrants further investigation of the influence of optical alignment. The external target is deliberately misaligned by an angle θ, and a SM signal is collected over a 500 μm translational scan. Fig. 7(a) illustrates (to scale) a ray trace up to the second RT for a target misalignment angle of $\theta = 2°$. It is evident that in such an asymmetric cavity, the feedback ray from the first RT is displaced further from the initial source compared to the feedback from the second RT. This will cause the coupling strength from the second RT to be more robust to target misalignment. This effect remains true in general for all odd-numbered versus even-numbered RTs, but higher-order contributions were observed to be much weaker and are not considered in this work [47, 48].

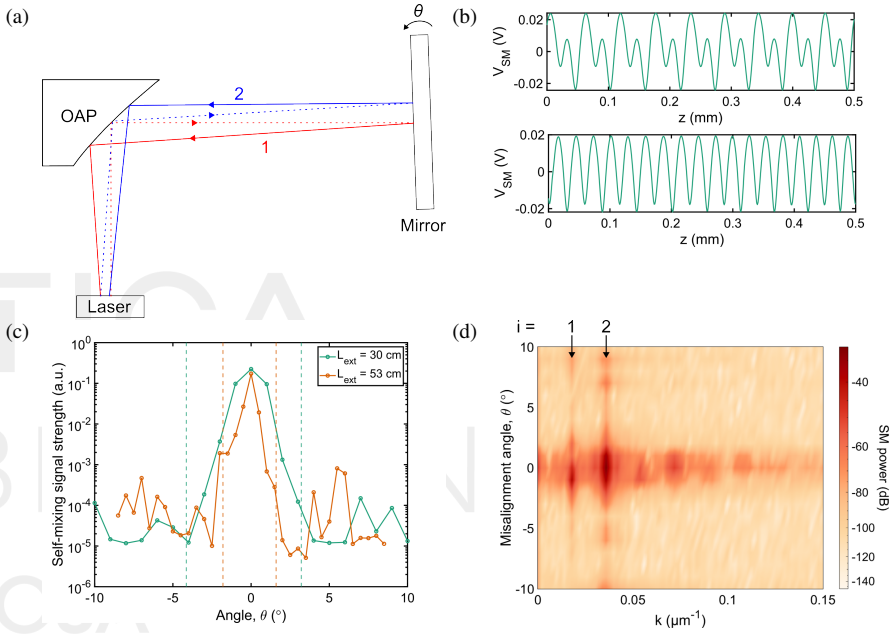

Fig. 7. (a) Ray tracing of the optical setup for a misaligned external target. The red trace corresponds to the first round-trip beam, and the blue trace corresponds to the second round-trip beam. The dotted portions of the path represent rays traveling away from the laser. The solid portions are rays traveling towards the laser. (b) Measured self-mixing voltage signals. The bottom signal is obtained when the mirror is rotated 2 degrees toward the laser. (c) Energy in the SM signal as a function of relative mirror angle for two different cavity lengths. The vertical dashed lines represent the angles that correspond to reflections incident at the physical edges of the OAP. (d) Spatial Fourier transform of the SM signal when $L_{30} = 30$ cm. The arrows indicate the spatial frequencies that correspond to the first and second round-trip.

Fig. 7(b) shows two SM signals obtained at an external cavity length of 30 cm. The top plot shows the case for when the target is close to perfectly aligned, and the contribution from the first and second RTs are comparable. The bottom plot was obtained by misaligning the mirror 2° off normal, which results in a SM signal that is dominated by the second RT as indicated by the near-$\lambda/4$ periodicity. Although it was left out in the analysis performed in Section 2 for simplicity, in general there can be additional phase offsets between each round-trip due to varied propagation lengths in an imperfectly aligned system. Data was collected across a range of misalignment angles from $-10°$ to $10°$, and the total energy in the SM signal is plotted for two external cavity lengths, $L_{\text{ext}} = 30$ cm and $L_{\text{ext}} = 53$ cm (Fig. 7(c)). The vertical dashed lines

correspond to the mirror angles that would result in the initial ray walking off the boundaries of the OAP (which has inherent asymmetry). In contrast to SM interferometry with edge-emitting lasers, the SM signal strength from the VECSEL appears to be significantly tolerant to target misalignment. This is due to two reasons. First, the output coupler serves as a large flat mirror that the initial ray can reflect off of to undergo secondary RTs. Second, the high beam-quality reduces the diffraction loss in the external cavity that would otherwise significantly attenuate the power from the second RT. The contribution from the second RT can be seen in Fig. 7(d), where the spatial Fourier transform is plotted against the relative misalignment angles for the case of $L_{\text{ext}} = 30$ cm. The spatial frequency labeled $i = 2$ corresponds to the component that is periodic with $\lambda/4$, and remains relatively independent of the angle until it approaches the physical edges of the OAP. One interesting observation is the spectral broadening of the higher order RT components. We speculate that this is caused by, in part, the higher sensitivity of higher order bounces in generating regions of multistability for lower feedback levels C_i as suggested by the model in Fig. 3.

4.3. Observation of self-mixing enhanced voltage instability

For higher signal-to-noise ratios, and faster signal acquisition, it is customary to implement an optical chopper for lock-in detection in a THz SM interferometric system [2, 12]. However, in our experiments, we observed moments of enhanced noise at the modulation frequency regimes accessible by the optical chopper (< 1 kHz). To investigate this further, we monitored the terminal voltage of the device in the frequency domain via an oscilloscope. Without the presence of optical feedback, a particular tone at ~920 Hz was always visible, as shown in Fig. 8(a). This tone is caused by the mechanical resonance of the quartz output coupler, and can vary depending on the thermo-mechanical state of the device. However, when optical feedback is introduced, this tone is amplified, and additional harmonics are generated due to the nonlinearity introduced by self-mixing at large feedback levels (Fig. 8(b)).

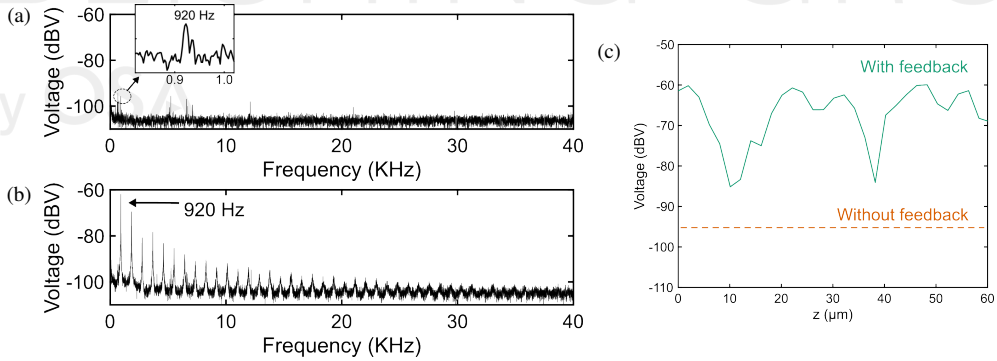

Fig. 8. (a) AC-coupled averaged voltage spectrum of the device biased at 410 mA without optical feedback. The inset shows a resonance at ~920 Hz. The spectrum is collected with a span of 40 KHz and a resolution bandwidth of 300 mHz. (b) Same conditions as (a), but with the presence of feedback. The harmonic tones are separated by 920 Hz. (c) Strength of the 920 Hz tone versus target mirror position. The orange dashed line shows the no feedback case as reference.

Additionally, we find that across all bias points and external cavity lengths, the presence of feedback always amplified the voltage instability. Fig. 8(c) plots the peak of the 920 Hz tone as the target mirror is swept across a half wavelength. Without feedback, the strength of the tone is measured to be -96 dBV with a 300 mHz resolution bandwidth. With feedback, the peak ranges from -85 dBV to -60 dBV, once again with a $\lambda/4$ periodicity. These results can be predicted based

on the model established in Section 2. The mechanical vibration of the output coupler can be represented as small perturbations to L_c. The corresponding perturbations to the SM voltage can be written as

$$\frac{\partial V_{SM}}{\partial L_c} \propto \frac{\partial g_{th}}{\partial L_c} = \frac{\partial g_{th}}{\partial \omega}\frac{\partial \omega}{\partial L_c}, \tag{14}$$

where

$$\frac{\partial g_{th}}{\partial \omega} = \frac{\partial g_{th,0}}{\partial \omega} + \frac{2}{\xi}\sum_{i=1}^{n} i\kappa_i \tau_{ext}\sin(i\phi_{FB}), \tag{15}$$

and

$$\frac{\partial \omega}{\partial L_c} = -\frac{2\omega/c}{2L_c/c + \tau_{MS} + \sum_{i=1}^{n} i\kappa_i \tau_{ext}\cos(i\phi_{FB})}. \tag{16}$$

The first term in Eq. (15) corresponds to the changes in threshold gain due to perturbations in the emission frequency without feedback. This can come from the frequency dependence of the metasurface resonance, output coupler reflectance, and the material gain lineshape. The frequency instability due to L_c for various feedback conditions is given by Eq. (16) and can be experimentally observed [49]. The expression suggests that the frequency stability can always be made better or worse depending on the feedback phase. However, in the case of the voltage stability, the perturbations to the threshold gain and the emission frequency are coupled, resulting in a more complicated dynamic.

4.4. Weak and moderate feedback regimes

Due to the phenomenon observed in Section 4.3, it is important that any SM interferometric system using the QC-VECSEL is configured to measure its signals spectrally far from the mechanical noise regime. This is especially true for higher levels of feedback. One way to achieve this is via small-signal modulation of the current source. Because the intrinsic frequency of the laser is a function of injected current, modulating the current modulates the intrinsic phase, $\phi_0 = \omega_0 \tau_{ext}$. This, in turn, produces a modified SM voltage signal given by

$$V'_{SM} \propto \frac{2}{\xi}\frac{d\omega_0}{dI}\frac{\sum_{i=1}^{n} iC_i \sin(i\phi_{FB})}{1 + \sum_{i=1}^{n} iC_i \cos(i\phi_{FB} + \arctan(\alpha_{eff}))}\Delta I. \tag{17}$$

While V_{SM} is a signal produced by feedback induced changes in the threshold gain, V'_{SM} is the signal produced by feedback induced changes in the differential resistance associated with photon-assisted transport. We modulate the current source by 0.80 mA peak-to-peak at 100 kHz (limited by the operating range of the lock-in amplifier). This current modulation corresponds to a frequency modulation of ~13.5 MHz/mA [49] of the laser mode. At an external cavity length of 61 cm, this corresponds to a phase modulation of $\Delta\phi_0 = 0.09\pi$.

While this alternate measurement scheme was motivated by operating away from mechanical noise, it comes with two additional benefits. One, modulation at higher frequencies allows faster lock-in detection and faster data acquisition rates. Two, signals corresponding to the moderate feedback regime become easily identifiable due to infinite discontinuities in differential resistance at the jump points (see Fig. 3). Fig. 9(a) shows an SM signal collected in the weak feedback regime, and one collected in the moderate feedback regime. The feedback level was controlled via crossed polarizers, allowing for additional RT field attenuation, ϵ_a, all the way down to the noise floor. Fig. 9(b) plots the maximum slope of the SM signal as the feedback level is gradually increased. The curvature follows from Eq. (17), but eventually saturates due to the discrete step size in z. Nevertheless, since our step size is much smaller than the periodicity ($\Delta z = 1$ μm), it allows us to easily identify excursions into the moderate feedback regime. We find that despite the large reflectance of the output coupler, the VECSEL is susceptible to moderate levels of

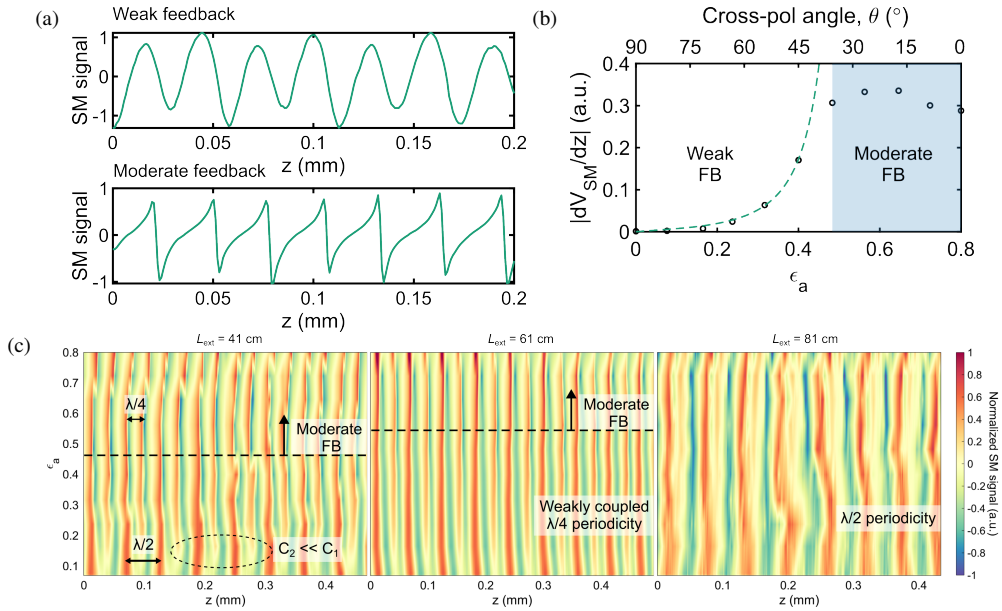

Fig. 9. (a) Measured self-mixing signals according to Eq. (17) in the weak feedback regime and the moderate feedback regime. (b) Maximum differential voltage as a function of field attenuation. The dashed curve show a trajectory according to Eq. (17). The blue shaded region corresponds to the moderate feedback regime. (c) Color plots of the SM signal for various levels of additional field attenuation via crossed-polarizers. The horizontal dashed lines indicate the approximate border between weak and moderate feedback. The dashed oval indicates a region where the feedback contribution from the second RT is much smaller compared to the first. The three color plots show data obtained for three different external cavity lengths: L_{ext} = 41 cm, L_{ext} = 61 cm, and L_{ext} = 81 cm.

feedback for cavity lengths up to 81 cm. Additionally, the relative feedback contributions from the first and second RT can vary significantly with attenuation and cavity length.

The color plots in Fig. 9(c) illustrate the obtained V'_{SM} signal for various levels of added attenuation. The three color plots, from left to right, show the case for L_{ext} = 41 cm, L_{ext} = 61 cm, and L_{ext} = 81 cm respectively. The horizontal dashed line indicate the border between weak and moderate feedback regimes. When the feedback level is high, and the cavity length is sufficiently short, the SM signals appear to be dominated by the second RT term. However, as further attenuation is added, C_1 becomes much larger than C_2, and the signal begins to recover $\lambda/2$ periodicity because the second RT term is attenuated by ϵ_a^2. Finally, as the external cavity length is further extended, the diffracted loss experienced by the second RT beam becomes large enough that its effects become extinguished. We also note that the device was biased near threshold, but these trends were similar across different bias points of the laser. These color plots exemplify the distinct behavior of a QC-VECSEL SM interferometer under various feedback conditions. Many of the well-developed analytical and analog processing techniques only work when higher-order RT reflections can be ignored [2, 12, 40, 50–53]. Therefore, extra care must be taken in the interpretation and processing of SM signals acquired from these devices.

5. Conclusion

We report the first investigation of self-mixing in THz QC-VECSELs: new phenomenology is observed, and a steady-state theoretical model is presented to describe it. Specifically, multi-bounce self-mixing is found to be prevalent at a large range of feedback conditions — something that has not been reported in conventional ridge waveguide THz QCLs. This can be understood as a consequence of the VECSEL's excellent beam quality, large millimeter-scale emitting aperture, and the fact that the output coupler is a large flat mirror which allows multiple round trips to survive in the feedback cavity. These effects are well described by a modified Lang-Kobayashi steady-state model which includes multi-bounce feedback, which in turn allowed extraction of an effective value for the linewidth enhancement factor of the gain-loaded metasurface.

These studies suggest that this external cavity architecture comes with particular challenges associated with its sensitivity to feedback, and its effect on laser instabilities. Nonetheless, the QC-VECSEL has the potential to be a powerful SM sensor. The combination of excellent beam pattern with the ability to choose the output coupler reflectance, allows one to deliberately reach high feedback coupling strengths, and obtain the concomitant high sensitivity. Being able to modify the feedback sensitivity with choice of OC is a unique feature of the VECSEL and is a potential avenue for future study. Furthermore, QC-VECSELs have been shown to exhibit broadband single-mode tunability (~19%) by using ultrashort cavities with piezoelectrically tunable lengths [28, 29]. Such a laser is potentially equipped to perform broadband SM interferometry for hyperspectral or 3D depth resolved imaging, solid-state or multi-species gas-phase spectroscopy, and measurement of complex refractive indices in the THz band. The device may also serve as a versatile platform for self-characterization and studying feedback effects across the gain bandwidth.

Appendix: Parameters used in this work

Funding. This research was partially funded by a SURP grant from the Jet Propulsion Laboratory, by the National Science Foundation (2041165), and by the National Aeronautics and Space Administration (80NSSC22K1894). Daniel McGovern was partially funded by an Research Experiences for Undergraduates supplement on the aforementioned NSF grant, as well as a UCLA LAEP internship.

Acknowledgments. The authors are grateful to Christopher Curwen from JPL for assistance with the active material as well as valuable discussions on QC-VECSEL feedback. We also acknowledge Professor Frédéric Grillot from Institut Polytechnique de Paris for his counsel and valuable insights. Finally, special thanks to Eilam Morag from UCLA for helpful discussions in the theoretical modeling.

Disclosures. The authors declare no conflicts of interest.

References

1. P. Dean, Y. L. Lim, A. Valavanis, R. Kliese, M. Nikolić, S. P. Khanna, M. Lachab, *et al.*, "Terahertz imaging through self-mixing in a quantum cascade laser," Opt. Lett. **36**, 2587–2589 (2011).
2. A. Valavanis, P. Dean, Y. L. Lim, R. Alhathlool, M. Nikolic, R. Kliese, S. P. Khanna, *et al.*, "Self-Mixing Interferometry With Terahertz Quantum Cascade Lasers," IEEE Sensors J. **13**, 37–43 (2013).
3. M. Wienold, T. Hagelschuer, N. Rothbart, L. Schrottke, K. Biermann, H. T. Grahn, and H.-W. Hübers, "Real-time terahertz imaging through self-mixing in a quantum-cascade laser," Appl. Phys. Lett. **109**, 011102 (2016).
4. P. Dean, A. Valavanis, J. Keeley, K. Bertling, Y. Leng Lim, R. Alhathlool, S. Chowdhury, *et al.*, "Coherent three-dimensional terahertz imaging through self-mixing in a quantum cascade laser," Appl. Phys. Lett. **103**, 181112 (2013).
5. A. D. Rakić, T. Taimre, K. Bertling, Y. L. Lim, P. Dean, D. Indjin, Z. Ikonić, *et al.*, "Swept-frequency feedback interferometry using terahertz frequency QCLs: a method for imaging and materials analysis," Opt. Express **21**, 22194–22205 (2013).
6. F. P. Mezzapesa, L. L. Columbo, M. Brambilla, M. Dabbicco, M. S. Vitiello, and G. Scamarcio, "Imaging of free carriers in semiconductors via optical feedback in terahertz quantum cascade lasers," Appl. Phys. Lett. **104**, 041112 (2014).
7. T. Hagelschuer, M. Wienold, H. Richter, L. Schrottke, K. Biermann, H. T. Grahn, and H.-W. Hübers, "Terahertz gas spectroscopy through self-mixing in a quantum-cascade laser," Appl. Phys. Lett. **109**, 191101 (2016).

Table 1. Parameter symbols and their descriptions

Parameter symbol	Description	Units
Γ_{MS}	Metasurface reflection coefficient	1
Γ_{ext}	External target reflection coefficient	1
Γ_{OC}	Output coupler reflection coefficient	1
Γ_{eff}	Effective reflection coefficient	1
τ_{ext}	RT time of external feedback cavity	s
τ_{int}	RT time of VECSEL cavity	s
τ_{MS}	Metasurface group delay ($\tau_{\mathrm{MS}} = 2\pi\mathcal{L}(\omega)$)	s
ϕ_0	Intrinsic phase accumulation in external cavity, ($\phi_0 = \omega_0\tau_{\mathrm{ext}}$)	rad
ϕ_{FB}	Feedback phase accumulation in external cavity, $\phi_{\mathrm{FB}} = \omega\tau_{\mathrm{ext}}$	rad
ϵ_i	Field attenuation factor for the i^{th} round-trip	1
κ_i	Feedback strength for the i^{th} round-trip	1
α_{eff}	Effective linewidth enhancement factor of the metasurface	1
C_i	Feedback level for the i^{th} round-trip	1
L_{c}	VECSEL cavity length	m
L_{ext}	Length of the external feedback cavity	m
τ_{r}	Radiative photon lifetime of the metasurface	s
τ_{m}	Non-radiative photon lifetime of the metasurface	s
R_{MS}	Metasurface reflectance	1
R_{OC}	Output coupler reflectance	1
ξ	Effective gain interaction length of the metasurface	m
ω_0	Intrinsic frequency of the laser without optical feedback	rad/s
ω_{r}	Resonant frequency of the metasurface	rad/s
ω	Frequency of the laser with optical feedback	rad/s
g_{th}	Threshold gain of the laser with feedback	cm^{-1}
$g_{\mathrm{th},0}$	Threshold gain of the laser without feedback	cm^{-1}
V_{SM}	RT time of external feedback cavity	V

8. Y. Leng Lim, P. Dean, M. Nikolić, R. Kliese, S. P. Khanna, M. Lachab, A. Valavanis, *et al.*, "Demonstration of a self-mixing displacement sensor based on terahertz quantum cascade lasers," Appl. Phys. Lett. **99**, 081108 (2011).
9. M. C. Giordano, S. Mastel, C. Liewald, L. L. Columbo, M. Brambilla, L. Viti, A. Politano, *et al.*, "Phase-resolved terahertz self-detection near-field microscopy," Opt. Express **26**, 18423–18435 (2018).
10. P. Dean, O. Mitrofanov, J. Keeley, I. Kundu, L. Li, E. H. Linfield, and A. Giles Davies, "Apertureless near-field terahertz imaging using the self-mixing effect in a quantum cascade laser," Appl. Phys. Lett. **108**, 091113 (2016).
11. R. Degl'Innocenti, R. Wallis, B. Wei, L. Xiao, S. J. Kindness, O. Mitrofanov, P. Braeuninger-Weimer, *et al.*, "Terahertz Nanoscopy of Plasmonic Resonances with a Quantum Cascade Laser," ACS Photonics **4**, 2150–2157 (2017).
12. R. P. Green, J.-H. Xu, L. Mahler, A. Tredicucci, F. Beltram, G. Giuliani, H. E. Beere, and D. A. Ritchie, "Linewidth enhancement factor of terahertz quantum cascade lasers," Appl. Phys. Lett. **92**, 071106 (2008).
13. M. C. Cardilli, M. Dabbicco, F. P. Mezzapesa, and G. Scamarcio, "Linewidth measurement of mid infrared quantum

cascade laser by optical feedback interferometry," Appl. Phys. Lett. **108**, 031105 (2016).
14. J. Keeley, J. Freeman, K. Bertling, Y. L. Lim, R. A. Mohandas, T. Taimre, L. H. Li, *et al.*, "Measurement of the emission spectrum of a semiconductor laser using laser-feedback interferometry," Sci. Reports **7**, 7236 (2017).
15. M. Piccardo and F. Capasso, "Laser Frequency Combs with Fast Gain Recovery: Physics and Applications," Laser & Photonics Rev. **16**, 2100403 (2022).
16. M. Franckié, M. Bertrand, and J. Faist, "Sensitive dependence of the linewidth enhancement factor on electronic quantum effects in quantum cascade lasers," Appl. Phys. Lett. **122**, 021107 (2023).
17. R. Tkach and A. Chraplyvy, "Regimes of feedback effects in 1.5-μm distributed feedback lasers," J. Light. Technol. **4**, 1655–1661 (1986).
18. G. Agrawal, "Line narrowing in a single-mode injection laser due to external optical feedback," IEEE J. Quantum Electron. **20**, 468–471 (1984).
19. L. Goldberg, H. F. Taylor, A. Dandridge, J. F. Weller, and R. O. Miles, "Spectral Characteristics of Semiconductor Lasers with Optical Feedback," IEEE TRANSACTIONS ON MICROWAVE THEORY AND TECHNIQUES (1982).
20. L. Jumpertz, M. Carras, K. Schires, and F. Grillot, "Regimes of external optical feedback in 5.6 μm distributed feedback mid-infrared quantum cascade lasers," Appl. Phys. Lett. **105**, 131112 (2014).
21. X. Qi, K. Bertling, T. Taimre, G. Agnew, Y. L. Lim, T. Gillespie, A. Robinson, *et al.*, "Observation of optical feedback dynamics in single-mode terahertz quantum cascade lasers: Transient instabilities," Phys. Rev. A **103**, 033504 (2021).
22. H. Hübers, H. Richter, R. Eichholz, M. Wienold, K. Biermann, L. Schrottke, and H. T. Grahn, "Heterodyne Spectroscopy of Frequency Instabilities in Terahertz Quantum-Cascade Lasers Induced by Optical Feedback," IEEE J. Sel. Top. Quantum Electron. **23**, 1–6 (2017).
23. F. P. Mezzapesa, L. L. Columbo, M. Brambilla, M. Dabbicco, S. Borri, M. S. Vitiello, H. E. Beere, *et al.*, "Intrinsic stability of quantum cascade lasers against optical feedback," Opt. Express **21**, 13748–13757 (2013).
24. Y. Wu, C. A. Curwen, M. Shahili, J. L. Reno, and B. S. Williams, "RF Injection Locking of THz Metasurface Quantum-Cascade VECSEL," Laser & Photonics Rev. **17**, 2300007 (2023).
25. X.-G. Wang, B.-B. Zhao, Y. Deng, V. Kovanis, and C. Wang, "Nonlinear dynamics of a quantum cascade laser with tilted optical feedback," Phys. Rev. A **103**, 023528 (2021).
26. B. S. Williams, "Terahertz quantum-cascade lasers," Nat. Photonics **1**, 517–525 (2007).
27. L. Xu, C. A. Curwen, D. Chen, J. L. Reno, T. Itoh, and B. S. Williams, "Terahertz Metasurface Quantum-Cascade VECSELs: Theory and Performance," IEEE J. Sel. Top. Quantum Electron. **23**, 1–12 (2017).
28. A. D. Kim, C. A. Curwen, Y. Wu, J. L. Reno, S. J. Addamane, and B. S. Williams, "Wavelength Scaling of Widely-Tunable Terahertz Quantum-Cascade Metasurface Lasers," IEEE J. Microwaves **3**, 305–318 (2023).
29. C. A. Curwen, J. L. Reno, and B. S. Williams, "Broadband continuous single-mode tuning of a short-cavity quantum-cascade VECSEL," Nat. Photonics **13**, 855–859 (2019).
30. C. A. Curwen, A. D. Kim, B. S. Karasik, J. H. Kawamura, and B. S. Williams, "Optical injection locking of a THz quantum-cascade VECSEL with an electronic source," Opt. Lett. **48**, 3809–3812 (2023).
31. K. Petermann, *Laser Diode Modulation and Noise* (Springer Netherlands, Dordrecht, 1988).
32. R. Lang and K. Kobayashi, "External optical feedback effects on semiconductor injection laser properties," IEEE J. Quantum Electron. **16**, 347–355 (1980).
33. S. Han, K. Bertling, P. Dean, J. Keeley, A. D. Burnett, Y. L. Lim, S. P. Khanna, *et al.*, "Laser Feedback Interferometry as a Tool for Analysis of Granular Materials at Terahertz Frequencies: Towards Imaging and Identification of Plastic Explosives," Sensors **16**, 352 (2016).
34. Y. L. Lim, T. Taimre, K. Bertling, P. Dean, D. Indjin, A. Valavanis, S. P. Khanna, *et al.*, "High-contrast coherent terahertz imaging of porcine tissue via swept-frequency feedback interferometry," Biomed. Opt. Express **5**, 3981–3989 (2014).
35. K. Vahala, L. C. Chiu, S. Margalit, and A. Yariv, "On the linewidth enhancement factor α in semiconductor injection lasers," Appl. Phys. Lett. **42**, 631–633 (1983).
36. N. Kumazaki, Y. Takagi, M. Ishihara, K. Kasahara, A. Sugiyama, N. Akikusa, and T. Edamura, "Detuning characteristics of the linewidth enhancement factor of a midinfrared quantum cascade laser," Appl. Phys. Lett. **92**, 121104 (2008).
37. G. Acket, D. Lenstra, A. Den Boef, and B. Verbeek, "The influence of feedback intensity on longitudinal mode properties and optical noise in index-guided semiconductor lasers," IEEE J. Quantum Electron. **20**, 1163–1169 (1984).
38. T. Taimre and A. D. Rakić, "On the nature of Acket's characteristic parameter C in semiconductor lasers," Appl. Opt. **53**, 1001–1006 (2014).
39. D. M. Kane and K. A. Shore, *Unlocking Dynamical Diversity: Optical Feedback Effects on Semiconductor Lasers* (John Wiley & Sons, 2005).
40. S. Donati, "Developing self-mixing interferometry for instrumentation and measurements," Laser & Photonics Rev. **6**, 393–417 (2012).
41. Y. Yu, J. Xi, J. F. Chicharo, and T. M. Bosch, "Optical Feedback Self-Mixing Interferometry With a Large Feedback Factor C : Behavior Studies," IEEE J. Quantum Electron. **45**, 840–848 (2009).
42. C.-M. Ri, C.-H. Kim, Y.-N. Oh, and S.-C. Kim, "Immediate estimation of feedback factor and linewidth enhancement factor from measured self-mixing signals under moderate or strong regime," Meas. Sci. Technol. **31**, 065204 (2020).
43. C. A. Curwen, S. J. Addamane, J. L. Reno, M. Shahili, J. H. Kawamura, R. M. Briggs, B. S. Karasik, and B. Williams,

"Thin THz QCL active regions for improved continuous-wave operating temperature," AIP Adv. **11**, 125018 (2021).
44. J. Keeley, K. Bertling, P. L. Rubino, Y. L. Lim, T. Taimre, X. Qi, I. Kundu, *et al.*, "Detection sensitivity of laser feedback interferometry using a terahertz quantum cascade laser," Opt. Lett. **44**, 3314–3317 (2019).
45. S. Kohen, B. S. Williams, and Q. Hu, "Electromagnetic modeling of terahertz quantum cascade laser waveguides and resonators," J. Appl. Phys. **97**, 053106 (2005).
46. C. A. Curwen, J. L. Reno, and B. S. Williams, "Terahertz quantum cascade VECSEL with watt-level output power," Appl. Phys. Lett. **113**, 011104 (2018).
47. D.-S. Seo, J.-D. Park, J. McInerney, and M. Osinski, "Multiple feedback effects in asymmetric external cavity semiconductor lasers," IEEE J. Quantum Electron. **25**, 2229–2238 (1989).
48. X. Cheng and S. Zhang, "Multiple selfmixing effect in VCSELs with asymmetric external cavity," Opt. Commun. **260**, 50–56 (2006).
49. C. A. Curwen, J. H. Kawamura, D. J. Hayton, S. J. Addamane, J. L. Reno, B. S. Williams, and B. S. Karasik, "Phase Locking of a THz QC-VECSEL to a Microwave Reference," IEEE Trans. on Terahertz Sci. Technol. **13**, 448–453 (2023).
50. T. Taimre, M. Nikolić, K. Bertling, Y. L. Lim, T. Bosch, and A. D. Rakić, "Laser feedback interferometry: a tutorial on the self-mixing effect for coherent sensing," Adv. Opt. Photonics **7**, 570 (2015).
51. R. Kliese, T. Taimre, A. A. A. Bakar, Y. L. Lim, K. Bertling, M. Nikolić, J. Perchoux, *et al.*, "Solving self-mixing equations for arbitrary feedback levels: a concise algorithm," Appl. Opt. **53**, 3723–3736 (2014).
52. Y. Gao, Y. Yu, J. Xi, Q. Guo, J. Tong, and S. Tong, "Improved method for estimation of multiple parameters in self-mixing interferometry," Appl. Opt. **54**, 2703–2709 (2015).
53. Y. Fan, Y. Yu, J. Xi, and J. F. Chicharo, "Improving the measurement performance for a self-mixing interferometry-based displacement sensing system," Appl. Opt. **50**, 5064–5072 (2011).